SPACE TELESCOPE SCIENCE INSTITUTE
Operated for NASA by AURA

Instrument Science Report WFC3 2005-11

Results of WFC3 Thermal Vacuum Testing - Image Stability

T.M. Brown
March 3, 2005

ABSTRACT

As part of the 2004 campaign of WFC3 thermal-vacuum tests, the image stability of both WFC3 channels (UVIS & IR) was measured over a wide range of environmental temperatures, simulating thermal variations that could occur in flight due to orbital occultations and slewing between hot and cold orientations. During orbital temperature cycles, the drift in the UVIS channel slightly exceeded its specification of 10 milliarcsec per 200 minutes, while the drift in the IR channel met its specification of 20 milliarcsec per 200 minutes. During large temperature slews, the UVIS channel drift exceeded its specification by a factor of 6, while the IR channel drift exceeded its specification by a factor of 3, and the alignment of the two channels diverged significantly. Alternative versions of these tests showed that much of this motion may be associated with the test apparatus instead of WFC3, but this is still under investigation.

Introduction

The thermal environment on HST varies significantly on a variety of timescales, due to orbital occultation and spacecraft orientation. These temperature variations can induce image drift in the scientific instruments, with two primary impacts on scientific observations: drift within an exposure will degrade the image resolution, while drift between exposures will hamper efforts to resample the point spread function (PSF) through dithering. For these reasons, the Contract End Item (CEI) specification for WFC3 image

stability calls for less than 10 mas (0.26 pixels) of drift in 200 min (2 orbits) on the UVIS channel, and less than 20 mas (0.15 pixels) of drift on the IR channel in 200 min.

The WFC3 image stability was tested on both channels during the thermal-vacuum campaign in the fall of 2004. Cryopanels placed around the instrument were used to simulate the temperature changes that would be seen in flight. Tests were done to simulate orbital variations (+/- 4 degrees C) in a hot HST environment (8.5 degrees C), orbital variations (+/- 4 degrees C) in a cold HST environment (-6.5 degrees C), transitions from hot to cold, and transitions from cold to hot. Two types of tests were performed to track the WFC3 image stability during these temperature variations, both involving long series of short WFC3 exposures interleaving the two WFC3 channels.

The primary test observed a compact source from the optical stimulus (CASTLE): a 10 micron fiber illuminated by a Tungsten lamp, giving a spot a few pixels wide on the WFC3 detectors (Figure 1); specifically, the spot had a FWHM of 1.9 pixels in the UVIS channel, corresponding to a FWHM of 0.6 pixels in the IR channel. The UVIS images were 10 sec exposures with a 400x400 pixel subarray and the F814W filter, to cut down on readout times. The IR images were RAPID=5 sample sequences with a 512x512 pixel subarray and the F126N filter, which corresponds to 8.2 sec of exposure time in each RAPID sequence. The filters were chosen to allow images with reasonable signal-to-noise ratio and to avoid saturation while viewing the same CASTLE source in the distinct WFC3 channels. Note that the first test run used the full 1024x1024 pixel frame in the IR images, but these longer exposures saturated because the CASTLE source was brighter than expected. The observations interleaved a series of images on each WFC3 detector, with no changes to the optical stimulus, and no changes to WFC3 other than the channel select mechanism (CSM). The “quad-cell” detector on CASTLE was used to record CASTLE motion, to enable subtraction of the CASTLE motion from the point source motion in the WFC3 images, with the intention of isolating motion intrinsic to WFC3.

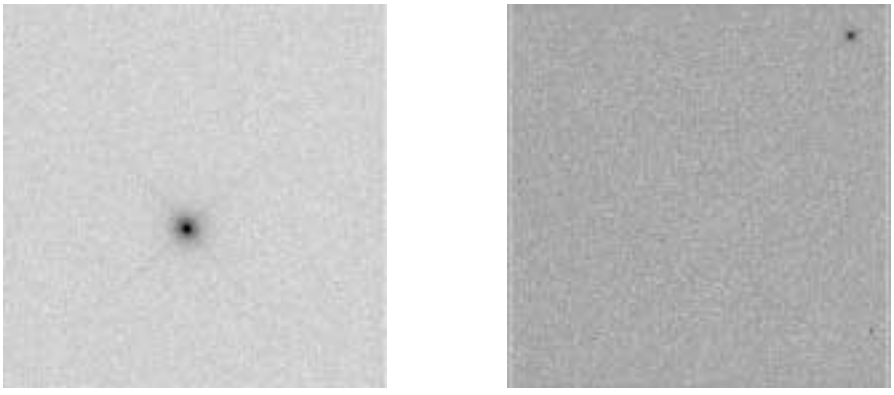

Figure 1: Inverse images from the UVIS channel (left; 400x400 pixel subarray) and IR channel (right; 512x512 pixel subarray) taken during the primary version of the WFC3 stability test, which observed an external point source.

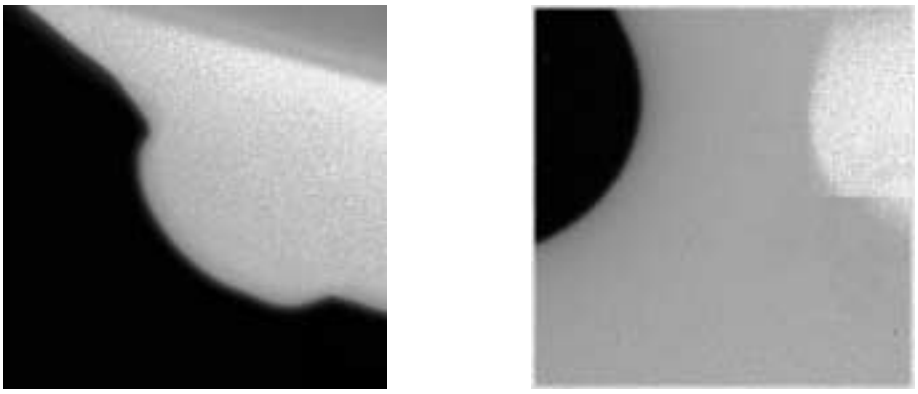

Figure 2: Inverse images from the UVIS channel (left; 1000x1000 pixel subarray) and IR channel (right; 512x512 pixel subarray) taken during the alternate version of the WFC3 stability test, which observed an extended source with the CSM placed in an intermediate state, partly blocking the beam.

Even with the CASTLE quad-cell data, it was difficult to completely rule out all sources of image drift external to WFC3, so an alternative version of the stability tests placed the CSM in an intermediate state that partly blocked each WFC3 channel (Figure 2). A flat-field extended source on CASTLE was then observed on both WFC3 channels, with no changes to the CASTLE or WFC3 (including the CSM) as the entire series of images was obtained. UVIS/F814W images were 1000x1000 pixel subarrays exposed for 40 sec, while IR/F126N images were 512x512 pixel subarrays with RAPID=8 sample sequences. Movement in the edges of the CSM provided an estimate of WFC3 motion utilizing indicators completely internal to WFC3, and including all components downstream of the pick-off mirror (POM). Motions in the POM, which would be important in flight, would not be detected by this alternative version of the stability test.

Analysis

Primary Test

The series of images in each test were analyzed using IDL software written for this purpose. The position of the point source was determined from a two-iteration centroid on a small background-subtracted subarray around the source. For the UVIS frames, the median was subtracted from the raw image, then a 20x20 pixel subarray around the approximate location of the source was used for a centroid, which gave a position used for extracting a new 20x20 pixel subarray and subsequent centroid. A similar process was used for the IR frames, except a difference image between the first and fourth reads was used instead of a single raw exposure, and the subarray used for the centroid iterations was only 5x5 pixels.

The CASTLE quadcell data are given in microns on the quadcell detector (X_{QC}, Y_{QC}). The conversion to milliarcsec (mas) in the UVIS frame (X_{UVIS}, Y_{UVIS}) requires the following transformation:

$$X_{UVIS} = -2.5844\ X_{QC} - 2.5714\ Y_{QC} \quad (1)$$

$$Y_{UVIS} = +2.7560\ X_{QC} - 2.4128\ Y_{QC} \quad (2)$$

To compare all of the stability data in the same reference frame, the WFC3 IR data were first transformed from mas in the IR frame (X_{IR}, Y_{IR}) to microns on the quadcell detector (X_{QC}, Y_{QC}) using the following transformation:

$$X_{QC} = -0.1752\ X_{IR} - 0.1960\ Y_{IR} \quad (3)$$

$$Y_{QC} = +0.1752\ X_{IR} - 0.1960\ Y_{IR} \quad (4)$$

and then transformed to the mas on the UVIS detector using equations 1 & 2.

Figures 2 through 12 show the results of the stability tests performed using the standard methodology. For each test, two sets of 3-panel plots are shown. The top panel in each set of 3-panel plots shows the temperature on the UVIS evaporator; this temperature is available in the FITS file headers (keyword IUVEVAPT), and is a convenient indication of the temperature changes occurring in the WFC3 environment. A heat pipe draws heat from the UVIS detector to the radiator; the end of the heat pipe at the detector is the evaporator, while the end of the heat pipe at the radiator is the condensor. The middle and bottom panels in each set of 3-panel plots show the X & Y motion in the WFC3/UVIS frame for the UVIS detector, IR detector, and CASTLE. In the first set of 3-panel plots, the CASTLE motion is not subtracted from the WFC3 motion, while in the second set of 3-panel plots, motions are shown relative to the CASTLE. Note that there is no absolute position for any of these components (WFC3/UVIS, WFC3/IR, or CASTLE) and so the WFC3/UVIS and WFC3/IR detectors are forced to agree with the CASTLE position for the first image in each of the WFC3 channels.

Ideally, one would want the CASTLE motion to be smaller than 10 mas in 200 min, so that the measured WFC3 motion was not subject to a correction significantly larger than the signal we were trying to detect. In practice, the CASTLE was not sufficiently isolated from the changes in the thermal environment, and most of the measurements of WFC3 motion were subject to a large correction for CASTLE motion. That said, the WFC3 motion looked reasonable during orbital cycling: depending upon where one selects 200 min of data, the UVIS channel motion met or slightly exceeded the CEI specification of 10 mas of drift in 200 min, while the IR channel motion almost always met the CEI specification. The same cannot be said of the WFC3 motion during large thermal slews. In those slews, the UVIS channel showed motion approximately 6 times larger than the CEI specification of 10 mas in 200 min, while the IR channel showed motion approximately 3 times larger than the CEI specification of 20 mas in 200 min. Furthermore, the UVIS and IR channels diverged from each other during these thermal slews at the rate of approximately 10 mas in 200 min, and that divergence must have been internal to WFC3.

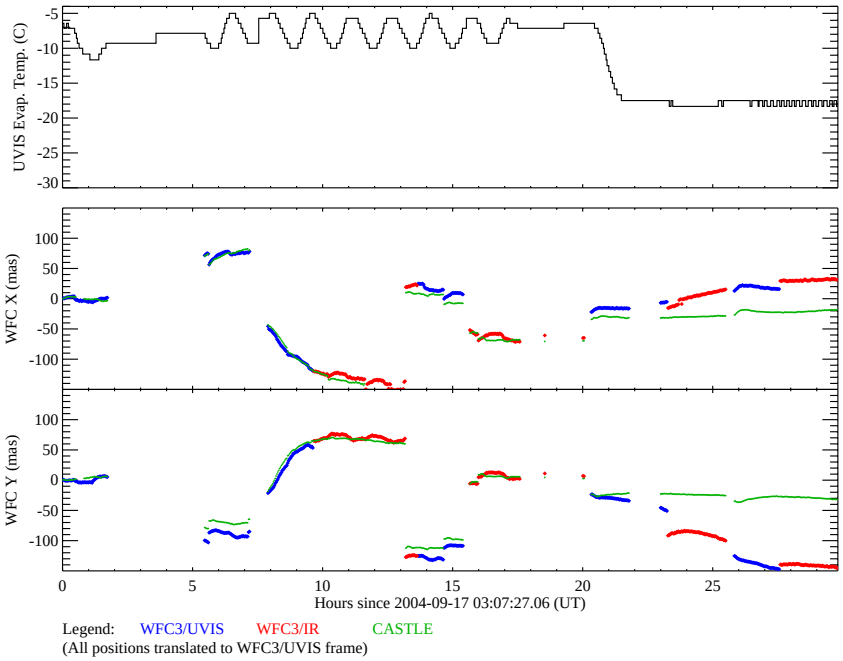

Figure 3a: The temperature of the UVIS evaporator (*top panel*), the motion along the x-axis (*middle panel*), and the motion along the y-axis (*bottom panel*). Motion is shown for the UVIS channel (*blue points*), IR channel (*red points*), and CASTLE (*green points*), all in the UVIS frame of reference. These data are from the first stability test, showing hot orbital cycling and a slew to a cold attitude. The instrument safed at approximately 22 hrs.

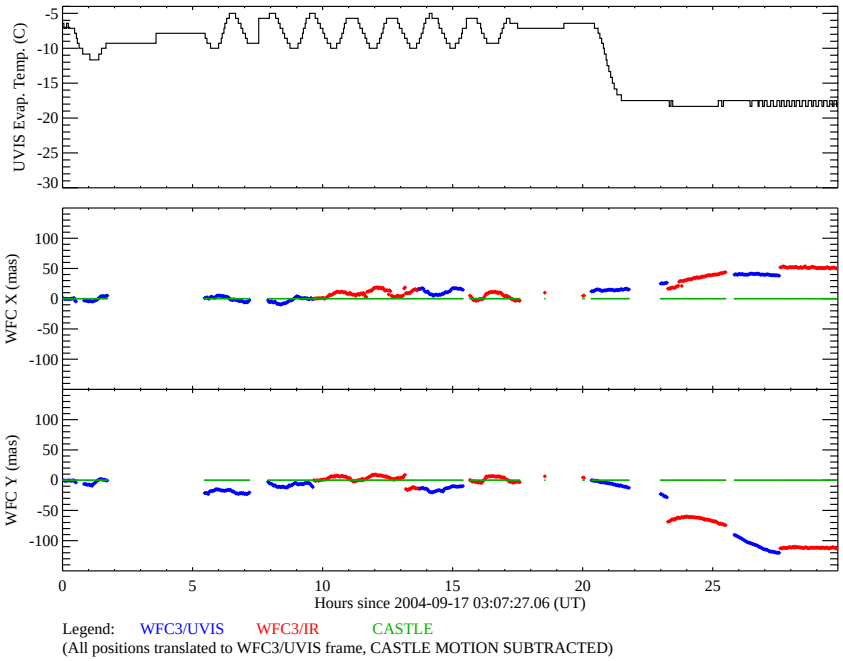

Figure 3b: The same information shown in Figure 3a, but now all motion is shown relative to the large motions inherent to the CASTLE.

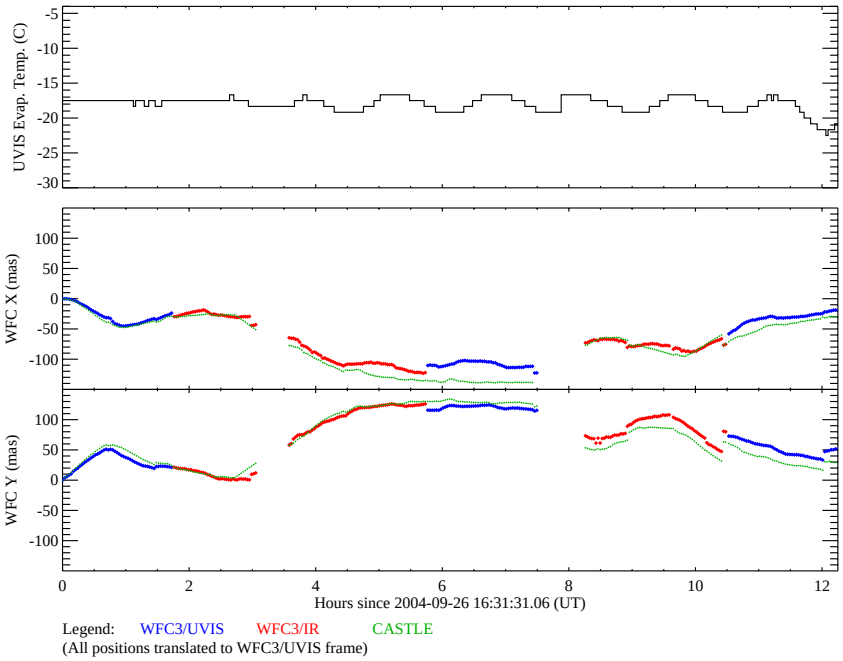

Figure 4a: The 2nd standard stability test, showing data from cold orbital cycling.

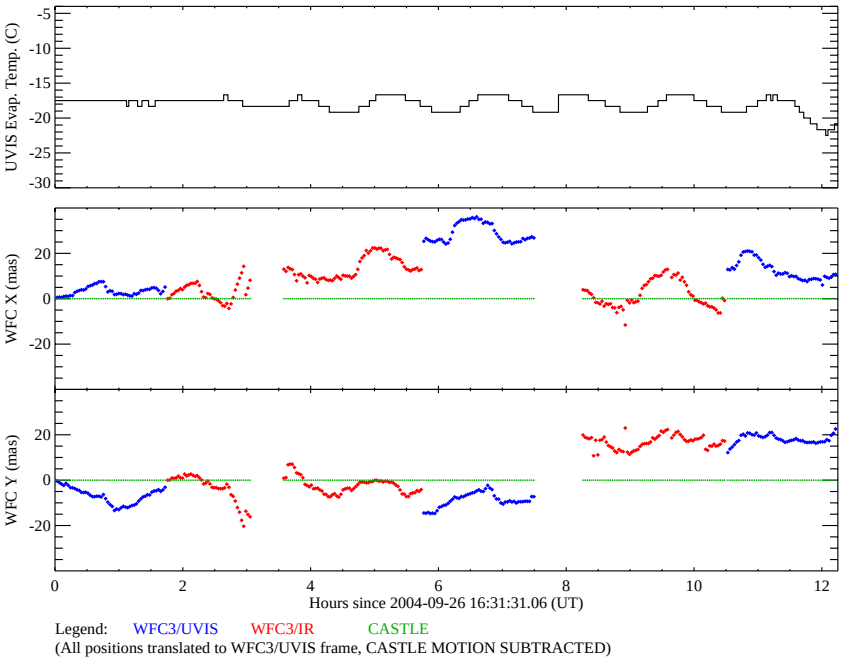

Figure 4b: The same data as in Figure 4a, but all motions are relative to the CASTLE motion.

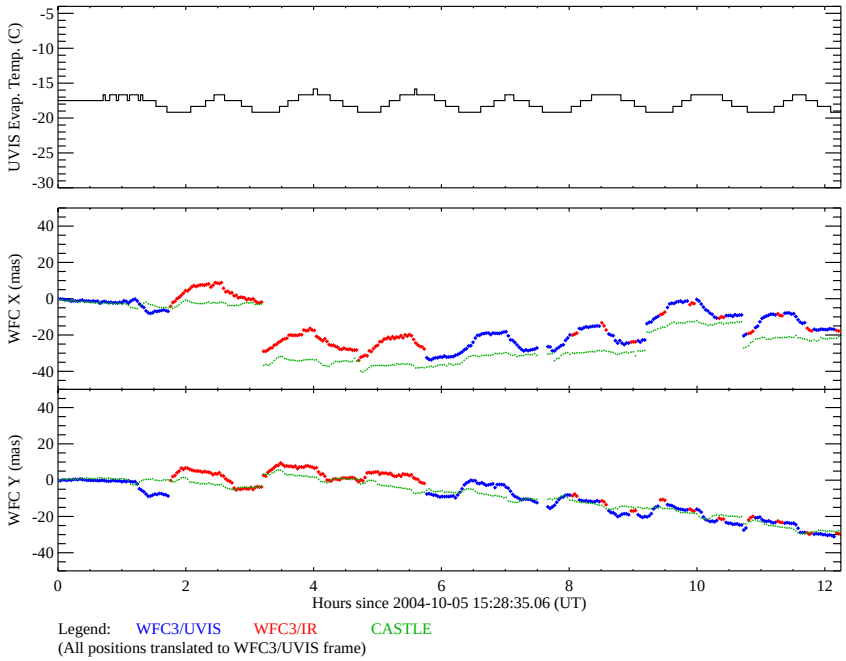

Figure 5a: The 3rd standard stability test, showing data for cold orbit cycling. As in the first test, the motion of the CASTLE is larger than desired. Ideally, the test would have small CASTLE motions (less than 10 mas) which could be subtracted from the WFC3 motions with a high degree of confidence.

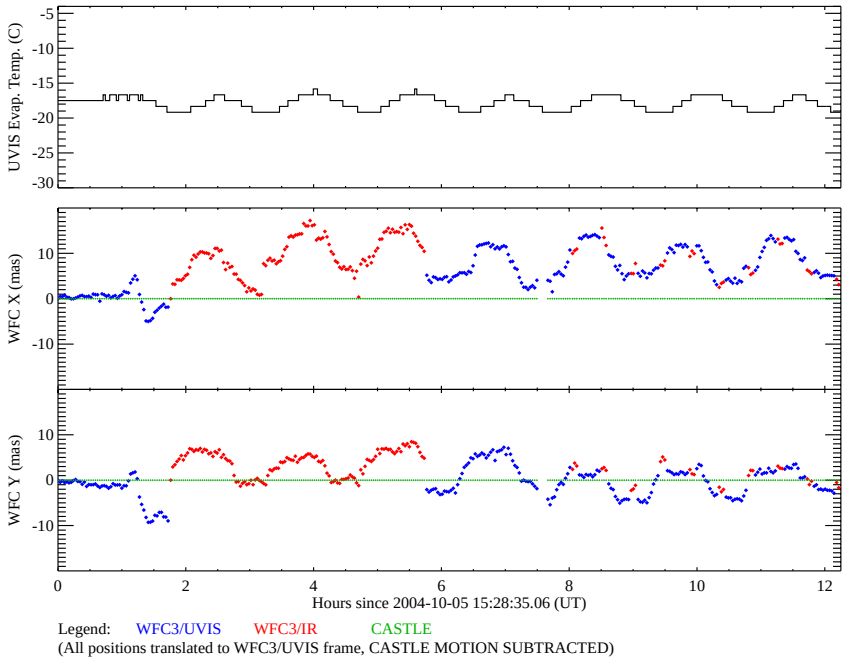

Figure 5b: The same data as in Figure 5a, but all motions are relative to the CASTLE motion.

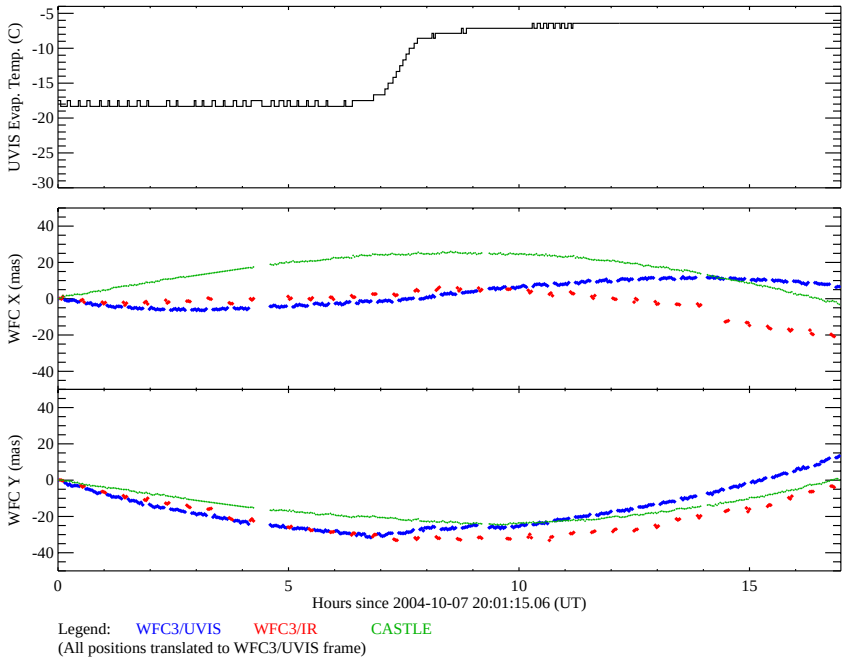

Figure 6a: The 4th standard stability test, showing data for a slew from a cold attitude to a hot altitude. The CASTLE motion is still fairly large, but more notable is the behavior of the two WFC3 channels, which diverge in their motion.

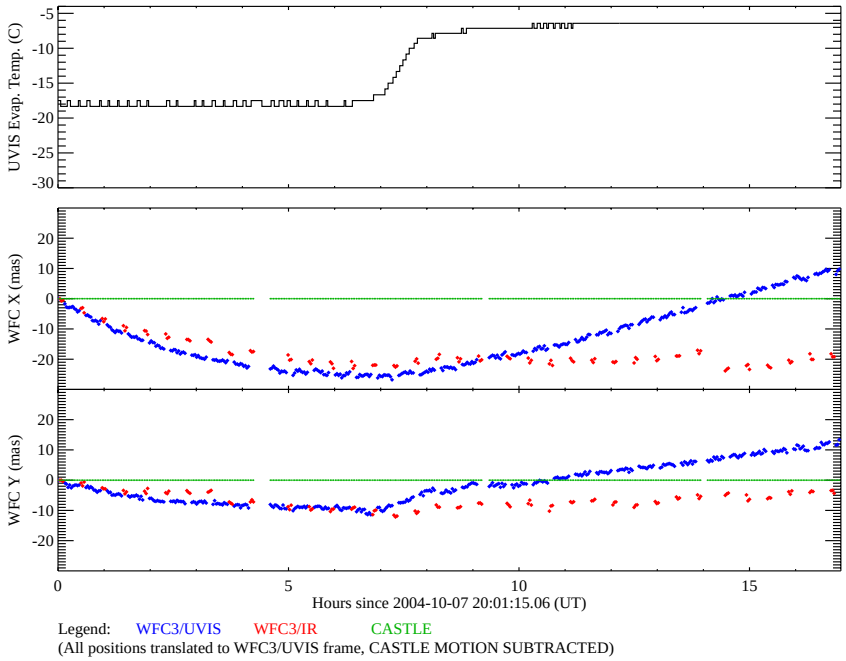

Figure 6b: The same data as in Figure 6a, but all motions are relative to the CASTLE motion.

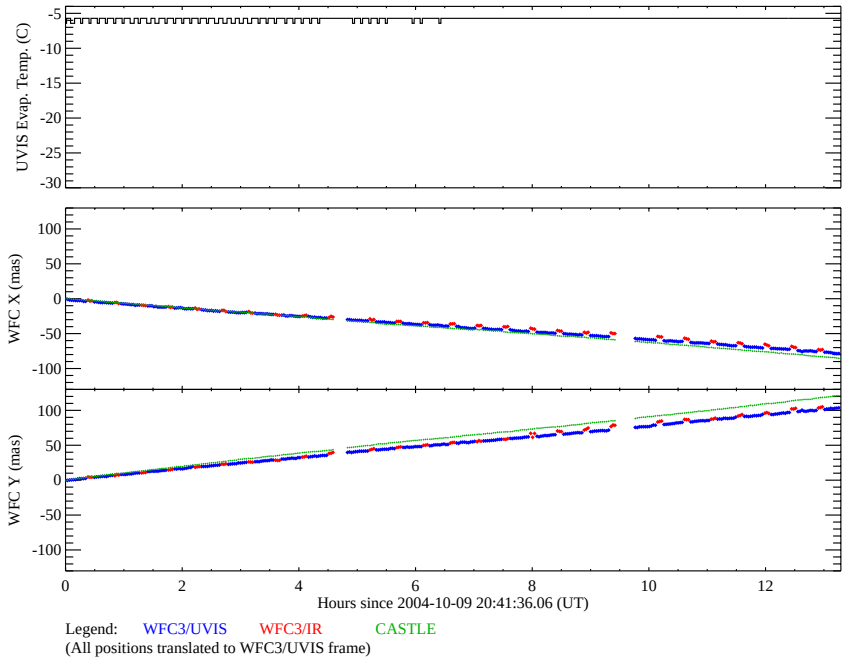

Figure 7a: The 5th standard stability test, showing data taken in a hot attitude but without orbital cycling. These data were taken while waiting for the environment and instruments to settle down before initiating the orbital cycling.

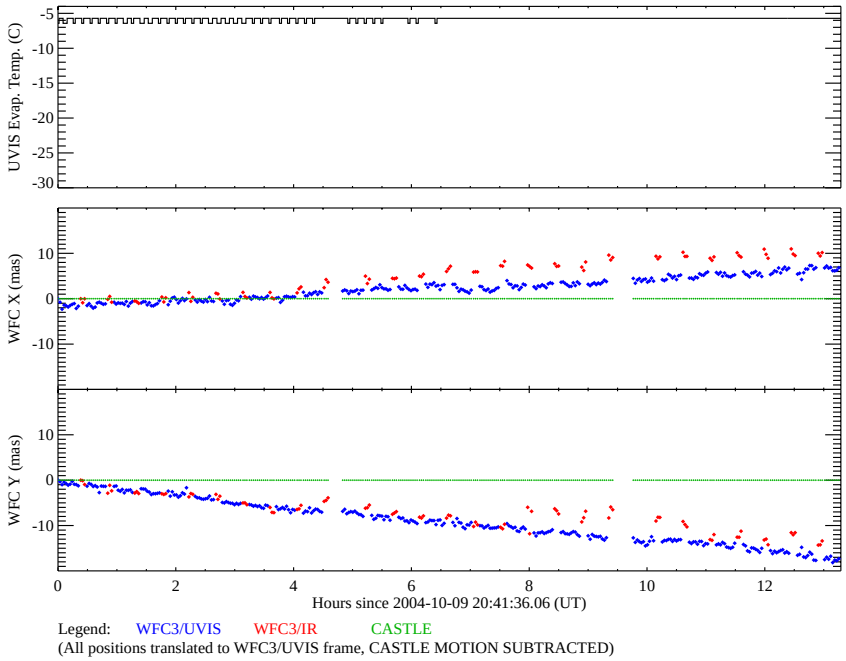

Figure 7b: The same data as in Figure 7a, but all motions are relative to the CASTLE motion.

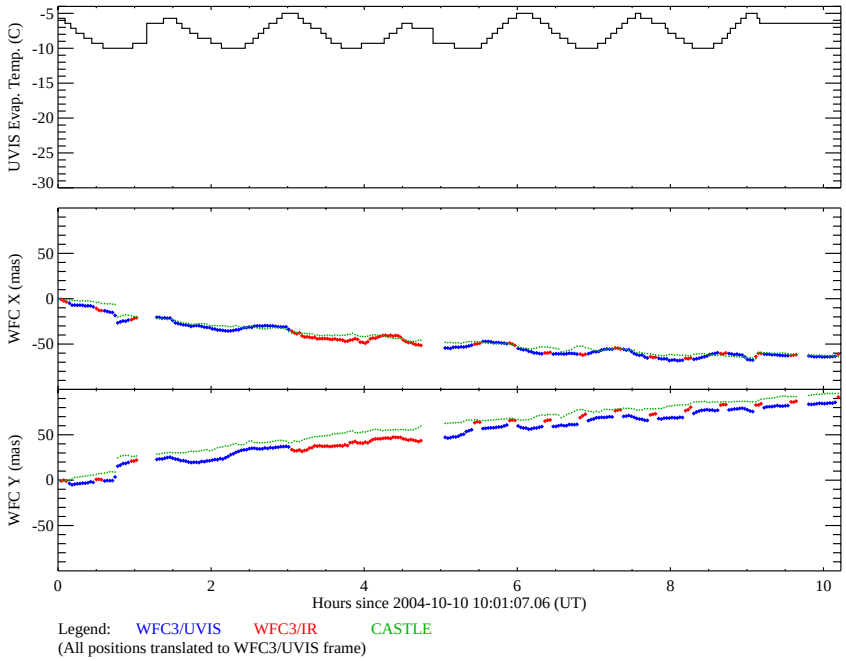

Figure 8a: The 6th standard stability test, showing data for hot orbit cycling. The CASTLE was still drifting significantly during this test.

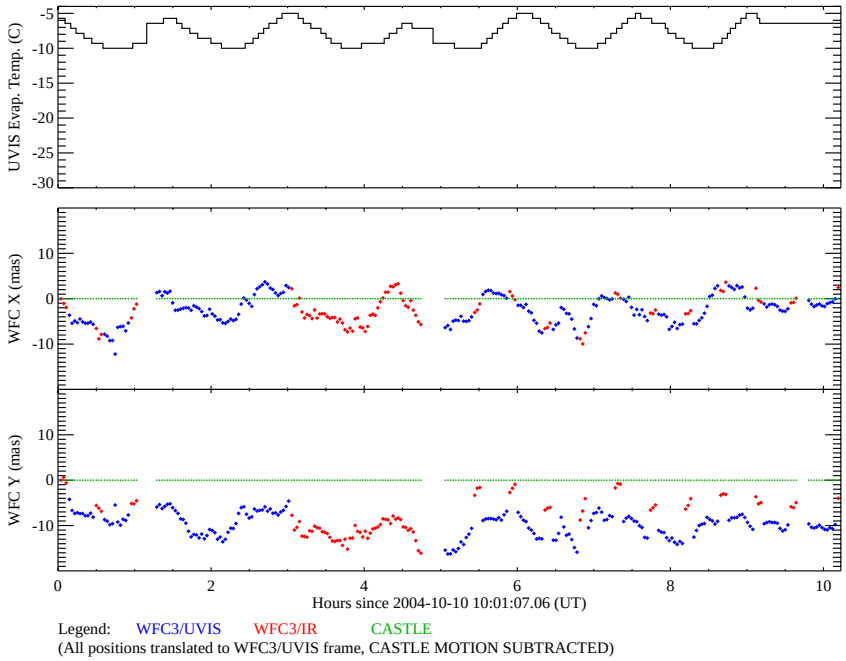

Figure 8b: The same data as in Figure 8a, but all motions are relative to the CASTLE motion.

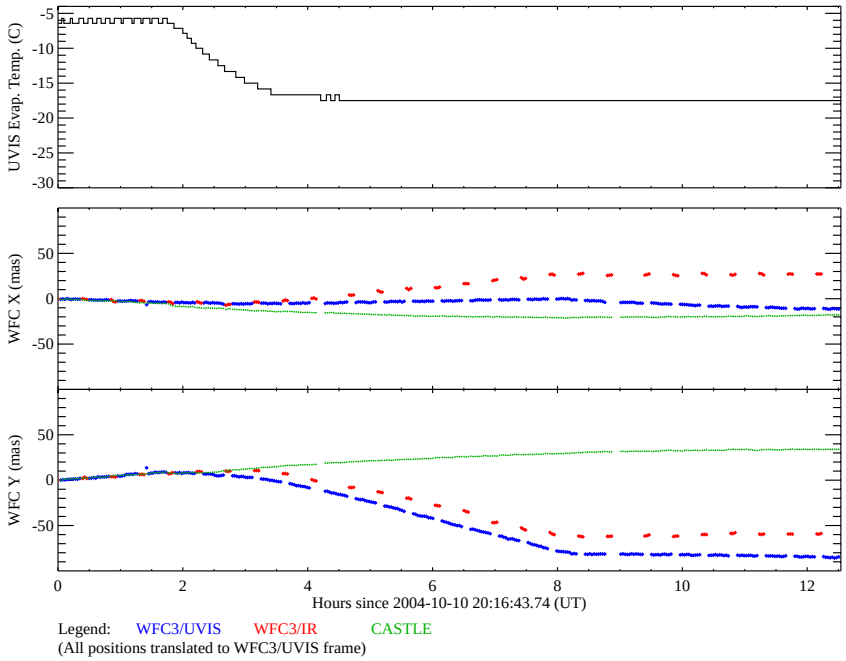

Figure 9a: The 7th standard stability test, showing data for a slew from a hot attitude to a cold attitude. Note the divergence of the two WFC3 channels.

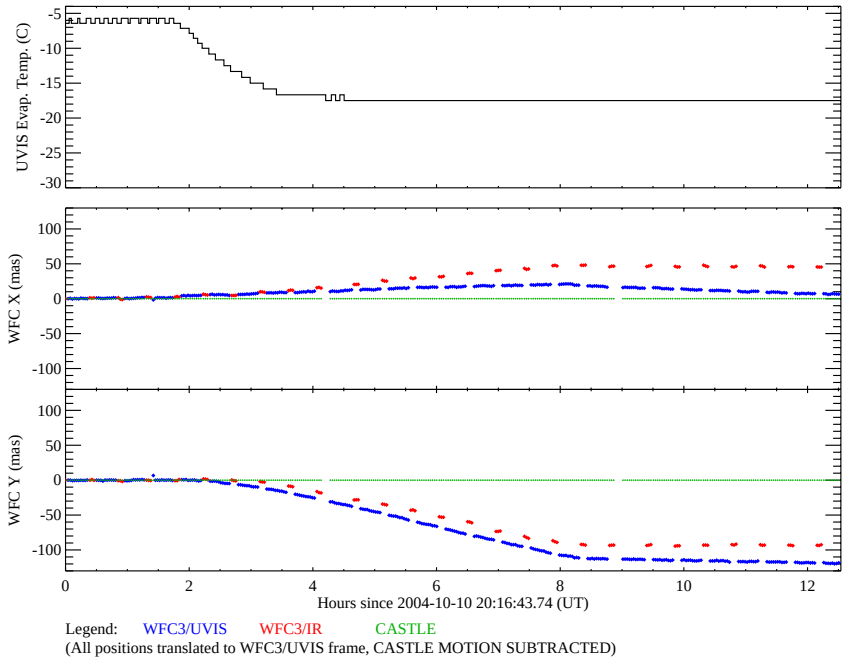

Figure 9b: The same data as in Figure 9a, but all motions are relative to the CASTLE motion.

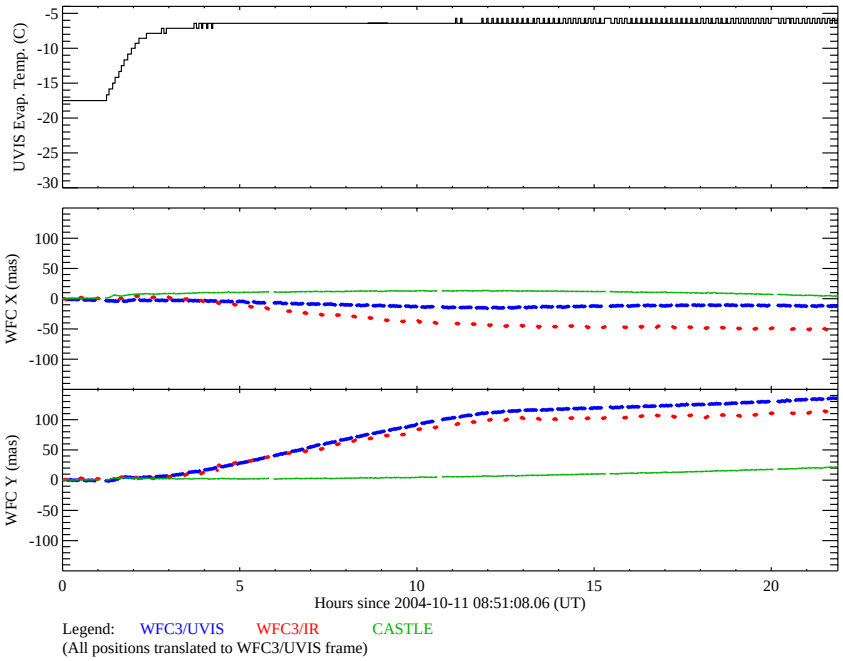

Figure 10a: The 8th standard stability test, showing data for a slew from a cold attitude to a hot attitude. Note the divergence of the two WFC3 channels.

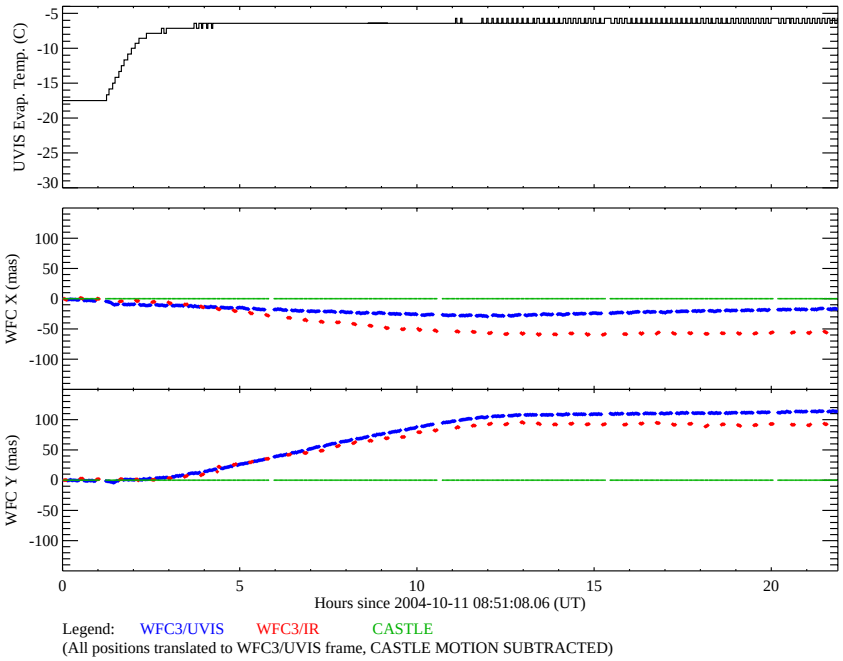

Figure 10b: The same data as in Figure 10a, but all motions are relative to the CASTLE motion.

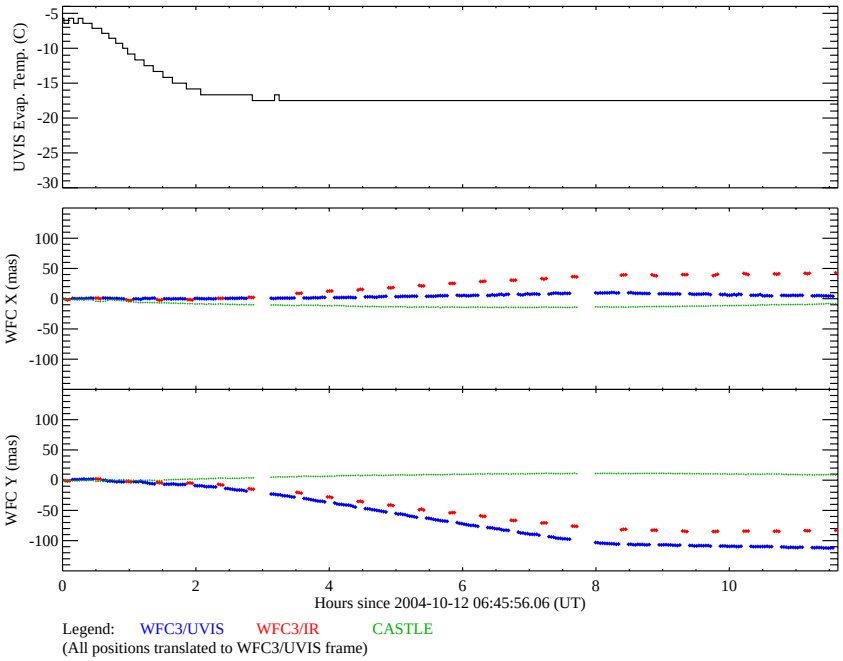

Figure 11a: The 9th standard stability test, showing data for a slew from a hot attitude to a cold attitude. Note the divergence of the two WFC3 channels.

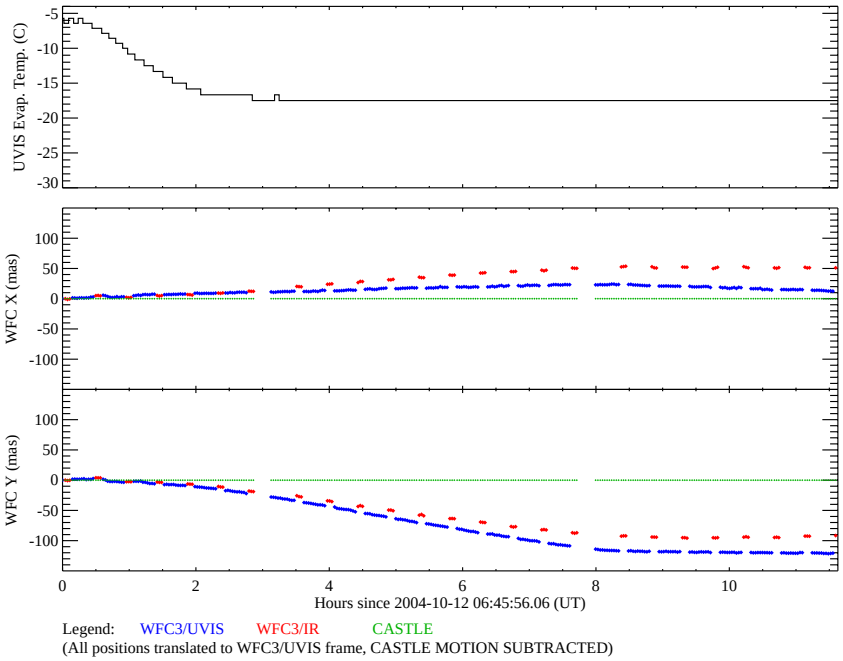

Figure 11b: The same data as in Figure 11a, but all motions are relative to the CASTLE motion.

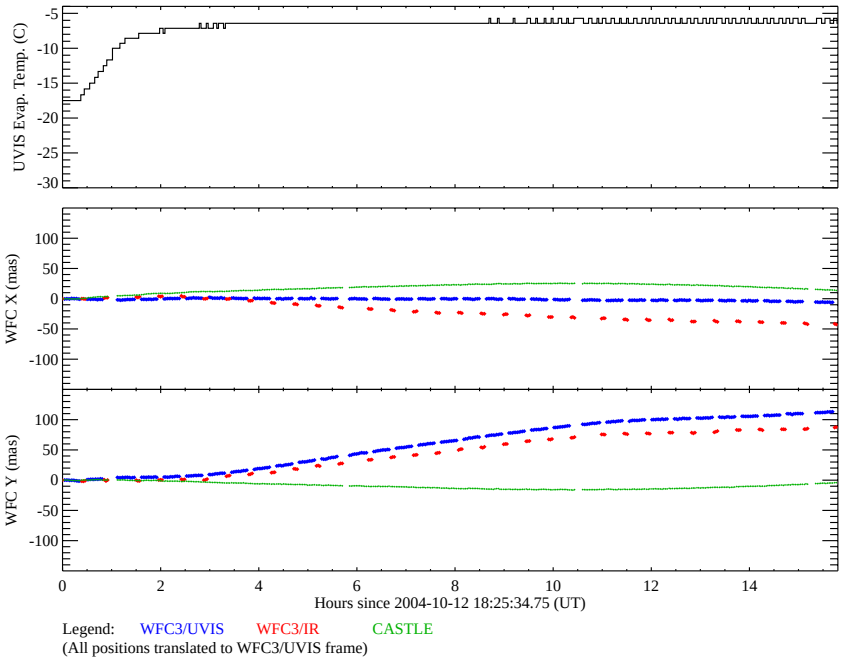

Figure 12a: The 10th standard stability test, showing data for a slew from a cold attitude to a hot attitude. Note the divergence of the two WFC3 channels.

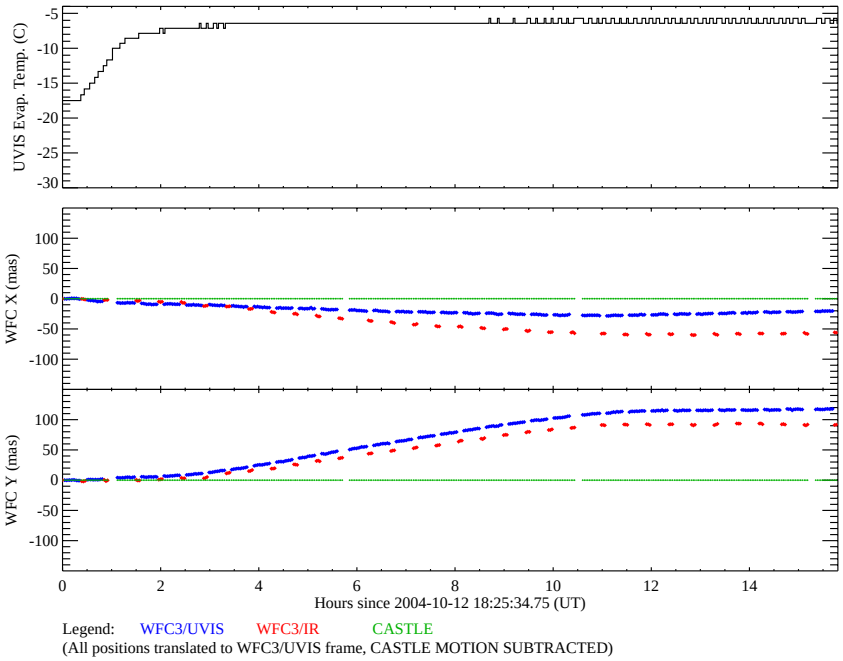

Figure 12b: The same data as in Figure 12a, but all motions are relative to the CASTLE motion.

Alternative (CSM) Test

The alternative test tracked motion in the shadow of the CSM, when it was placed in an intermediate position that partially blocked each of the WFC3 channels. The motion was tracked via cross-correlation, comparing the images in each channel to the first image in each channel, using regions of the image that spanned an edge in the CSM shadow. For the UVIS 1000x1000 pixel subarrays, a 20x80 pixel region was extracted at the location (740,195), and collapsed in X; cross-correlating all images against the first, using this collapsed region, gave the Y-offset as a function of time. For the X-offset as a function of time, a 80x20 pixel region was extracted at the location (330,590), collapsed in Y, and cross-correlated. For the IR 512x512 pixel subarrays, the subarray was first rotated by 25 degrees clockwise to give edges more closely aligned with image rows and columns. For the Y-offset as a function of time, a 15x40 pixel region was extracted at the location (30,317) in the rotated image, collapsed in X, and cross-correlated. For the X-offset as a function of time, a 40x15 pixel region was extracted at the location (230,507) in the rotated image, collapsed in Y, and cross-correlated. The resulting X & Y motion in the rotated frame was then rotated by 25 degrees counter-clockwise, to put the motion back in the original IR frame. Then, as done in the primary version of the stability tests, the IR motion in mas was transformed to the quadcell frame, in microns (using equation 2) and then transformed to the UVIS frame, in mas (using equation 1), so that the motions of both channels were given in the UVIS frame.

Figures 13 through 16 show the results of the stability tests using this alternative version (tracking the edges of the CSM shadow). Unlike Figures 3 through 12, here only a single 3-panel plot is shown for each stability test, because there is no CASTLE motion to subtract (all motions are completely internal to WFC3, but excluding any motion in the POM). The top panel in each figure shows the UVIS evaporator temperature. The middle panel shows the motion along the WFC3/UVIS x-axis, while the bottom panel shows the motion along the WFC3/UVIS y-axis. As before, the UVIS and IR data are shown in blue and red, respectively.

During orbital cycling, the motion in both the UVIS and IR channels were well within the CEI specifications. During the large thermal slews, the UVIS channel motion slightly exceeded the specification of 10 mas in 200 min, while the IR channel motion was less than the specification of 20 mas in 200 min. Because these motions were so much smaller than those in the primary test, these alternative tests might indicate that much of the motion in the primary tests was external, unless that motion was in the WFC3 POM. Note that the divergence between the two WFC3 channels was the same in both the primary and alternative versions of the tests, in terms of direction, magnitude, and timescale; compare Figure 11b to Figure 14, and Figure 12b to Figure 15. This is not surprising, given that this divergence must be completely internal to WFC3.

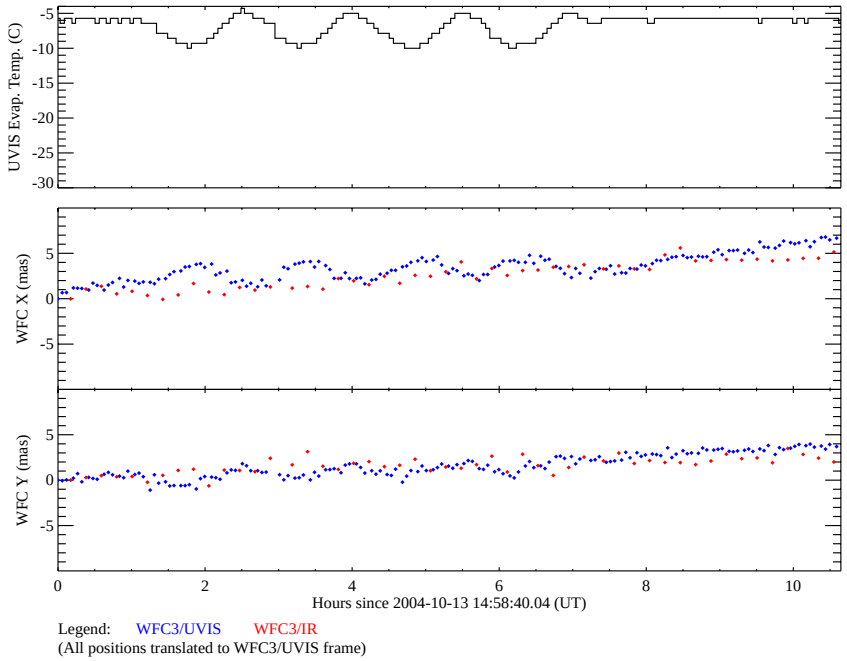

Figure 13: The temperature of the UVIS evaporator (*top panel*), the motion along the x-axis (*middle panel*), and the motion along the y-axis (*bottom panel*). Motion is shown for the UVIS channel (*blue points*) and IR channel (*red points*) in the UVIS frame of reference. These data are from the first run of the alternative stability test, tracking edges in the CSM shadow during hot orbit cycling. Motion is well within the CEI specifications.

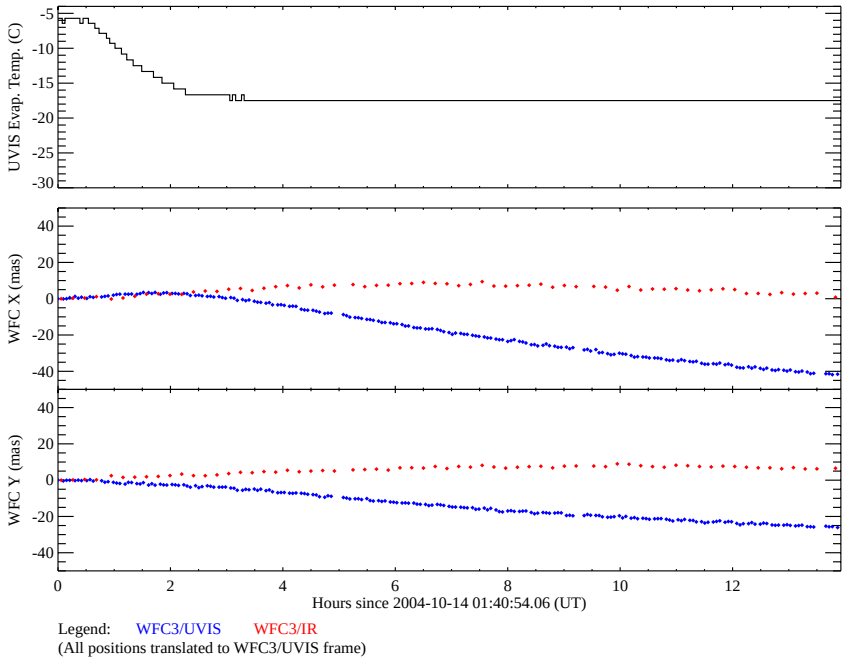

Figure 14: The second run of the alternative stability test, during a slew from a hot to a cold attitude. The channel deviation is the same as that in Figure 11b.

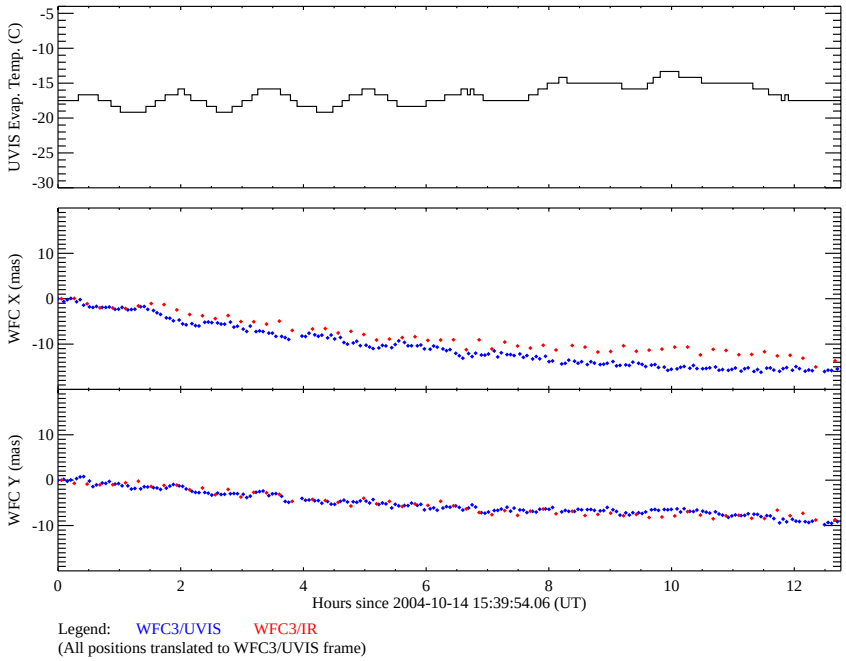

Figure 15: The third run of the alternative stability test, during cold orbit cycling. Again, the motion is well within the CEI specifications.

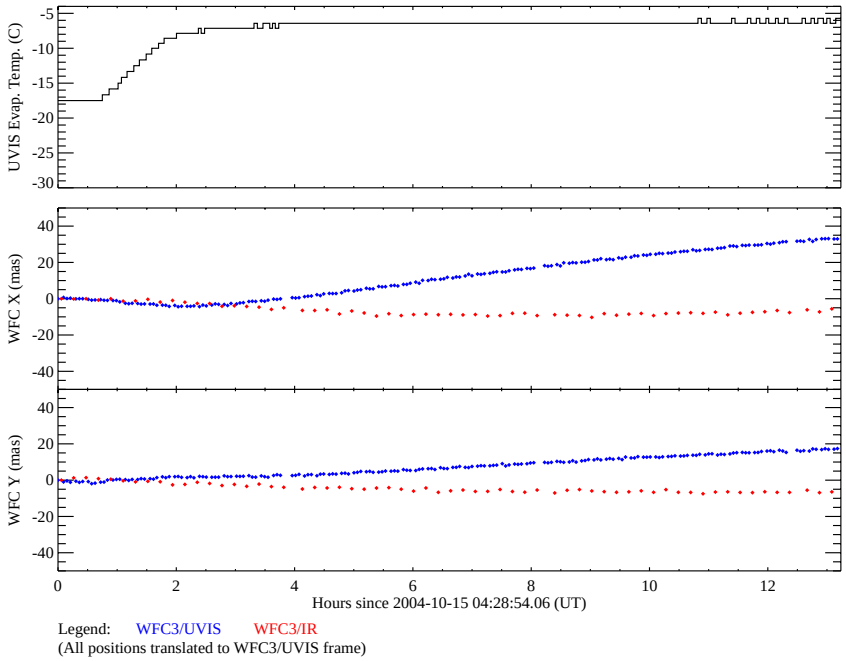

Figure 16: The fourth run of the alternative stability test, during a slew from a cold attitude to a hot attitude. The channel deviation is the same as that in Figure 12b.

Conclusions

The WFC3 stability tests showed good performance during orbital thermal variations. In the standard version of the stability tests (tracking the motion of an external point source), the UVIS channel showed motion at the level of the CEI specification of 10 mas in 200 min, and sometimes exceeded this specification slightly, while the IR channel showed motion that was usually within the CEI specification of 20 mas in 200 min. In the alternative version of the stability tests (tracking the shadow of the CSM while illuminated by an external flat-field source), the UVIS and IR channels both showed motions smaller than the CEI specifications. It is unclear how much of the motion in the primary tests was due to components external to WFC3; the alternative tests, which tracked motion purely internal to WFC3, showed much smaller motions than the primary tests, but were insensitive to motion of the POM.

The stability tests implied that WFC3 might not meet the CEI specifications during large thermal slews: the UVIS channel exceeded its specification by a factor of approximately six, while the IR channel exceeded its specification by a factor of approximately three. Again, some of this motion may be external to WFC3. The alternative stability tests showed much smaller motions during these large thermal slews, with the UVIS channel showing slightly larger motions than the CEI specification, and the IR channel showing motions within the CEI specification. During large thermal slews, the UVIS and IR channels diverged from each other in a consistent way regardless of test methodology.

If all of the motions seen in both the primary and alternative tests were intrinsic to WFC3, and if the large thermal slews in these tests were representative of flight conditions, the motions seen during these tests could cause a significant degradation of image quality during flight, both in the quality of individual exposures and in the quality of images coadded under PSF-resampling dithering schemes. The longest CCD exposures on HST are typically close to 1300 sec (half of the visibility period in a given orbit), due to the trade-off between cosmic rays and read noise (too many reads in an orbit increases the read noise above the sky noise, while only one read in an orbit results in an image with too many cosmic rays). Four hours into the last test slewing from a hot attitude to a cold attitude (Figure 11b), the UVIS channel moved 17% of a pixel in Y and 2.3% of a pixel in X over a 1300 sec span. This would cause a significant smearing of the PSF in an individual exposure. As for PSF resampling, there would also be a significant degradation. A typical dithering scheme is to use a four-point dither pattern spanning a two-orbit visit, with dither positions of (0,0), (n+1/2,0), (0,n+1/2), and (n+1/2,n+1/2), in pixels, where n is some small integer. Such a scheme allows the PSF to be sampled at twice the pixel sampling intrinsic to the detector. However, the UVIS channel drifted 1.5 pixels in Y and 0.2 pixels in X over a 3.2 hour visit that began 4 hours into the thermal conditions of Figure 11b; such a large movement would defeat any attempts to resample the PSF at half-pixel intervals. It is worth stressing, though, that further tests are required to see if the motions described herein were intrinsic to WFC3 and representative of flight conditions.